

# Doped Holographic Superconductors in Gubser-Rocha model

Ziyi Zhao <sup>a</sup>, Wenhe Cai <sup>a,b,\*</sup>, Shuta Ishigaki <sup>a</sup>

<sup>a</sup>*Department of Physics, Shanghai University, Shanghai 200444, China*

<sup>b</sup>*Shanghai Key Laboratory of High Temperature Superconductors, Department of Physics, Shanghai University, Shanghai 200444, China*

**ABSTRACT:** We construct a doped holographic superconductor in the Gubser-Rocha model, and realize a superconducting dome in the middle of the temperature-doping phase diagram. From the numerical observation for the coupling dependence of the phase diagram, we find that the coupling between the two gauge fields plays a crucial role in the formation of dome. We also analytically calculate the DC conductivity of the normal phase of the system in the momentum dissipation, which is proportional to temperature. The AC conductivity is calculated numerically. There is a symmetry between  $\sigma_A$ ,  $\sigma_B$  and  $\gamma$  with specific doping parameter  $x$  in normal phase, and this symmetry continues to exist with the momentum dissipation.

**keywords:** AdS-CFT Correspondence, High- $T_c$  superconductor, AC/DC conductivities, Gubser-Rocha geometry

---

\* whcai@shu.edu.cn

## I. INTRODUCTION

The thermodynamic and transport properties of non-Fermi liquids such as high temperature cuprate superconductors are strongly different from those described by the standard Fermi liquid theory[1]. There is still no satisfactory theoretical framework to describe them so far. The AdS/CFT correspondence, also known holographic duality[2–4], provides a useful tool for high- $T_c$  cuprate strange metals and other strongly correlated systems[5–7]. Recently, holographic duality has brought some new breakthroughs in condensed matter physics, such as: holographic superconductivity model[8–10], strange metal[11, 12], linear resistivity[13, 14], Hall Angle[15, 16] and so on.

There are some similarities in the temperature-doped phase diagrams of many unconventional superconductors, such as high-temperature cuprates[10, 17, 18], with an antiferromagnetic phase, a superconducting phase, a metallic phase and a striped phase competing and coexisting with each other. How to construct a holographic theoretical model to reproduce and understand such a phase diagram becomes an important problem. In recent years, holographic two-current model has attracted attention[19–26]. It has been pointed out that the model has a corresponding Mott insulator[27–30], and there are two spintronic "up" and "down" currents which can be regarded as independent entities at low temperatures[24, 31, 32]. These models include two gauge fields in bulk describing the two currents of the dual boundary field theory. Two independent conserved currents are associated with two different chemical potentials or charged densities, and their ratio defines the "doping" variable  $x$ , i.e.  $x = \rho_A/\rho_B$ . Recently, Kiritsis et al.[20] added the related bulk fields dual to the operators of the boundary field theory to simulate the phase diagram that the normal phase, superconducting phase, antiferromagnetic phase and fringe phase compete with each other and coexist in the temperature-doped plane, in which the superconducting phase appears in the dome-shaped region in the middle of the phase plane. Ref.[21] introduces a neutral axion field of [33] to break the translational symmetry of the system, so that the normal phase has a finite DC conductivity distinguished from the superconducting phase. Their results also demonstrate that Kiritsis's superconducting dome still exists even with broken translational symmetry. Subsequent studies use this model to discuss the effects of quantum critical points on dome under hyperscaling violation geometry[22]. They reconsidered the role of the first class of charges with density  $\rho_A$  in the temperature-doping phase diagram to form the Mott insulator, and the second class of charges with density  $\rho_B$  to form additional charges by "doping".

On the other hand, previous studies construct holographic models with hyperscaling violating factor[34, 35]. Particularly, Gubser-Rocha model is characterized by the hyperscaling  $z \rightarrow \infty$  and Lifshitz exponents  $\theta \rightarrow -\infty$ . It implies the entropy is proportional to temperature near zero temperature with local quantum criticality[36]. It is similar to more realistic strange metals[37, 38]. In order to simulate a more realistic holographic superconductor, in this paper, we construct a holographic superconducting dome in Gubser-Rocha model with two charges. One kind of charge is non-movable, which contribute to the half filled state of Mott insulator. One kind of charge is movable, which contribute to the state near the Fermi surface. The ratio of these two charges is the doping parameter. When the ratio increases, there is a dome-shaped superconducting region which is experimentally observed. That is, the critical temperature rises first and then decreases with the increase of doping. In order to make conductivity realistic, we also introduce holographic superconductor with momentum dissipation by breaking translational symmetry[21, 39, 40]. By calculating the DC conductivity of our model, we prove that the normal phase of the model satisfies the linear- $T$  resistivity relation[13] in the presence of momentum dissipation. We also numerically calculate the AC conductivity[41–43] of the normal phase with momentum dissipation. We also calculate spin conductivity  $\gamma$  of our model, and as a result we observe behavior similar to the conductivity of Mott insulators.

This paper is organized as follows. In section 2, we set up the doped holographic superconductor, based on the Gubser-Rocha model with broken translational symmetry. In section 3, we obtain the linear- $T$  resistivity analytically and AC conductivities numerically in the normal phase in order to explore the two-current model. In section 4, the normal phase of the bulk system was observed to become unstable at  $T_c$ , then developing a nontrivial profile of the scalar field  $\chi$ , which means a superconducting phase transition. We study superconducting instability with the critical temperature  $T_c$  by numerically solving the motion equation of  $\chi$  in the normal phase background, and draw the superconducting dome phase in temperature-doping plane. We conclude with discussions at section 5.

## II. CONSTRUCTION OF THE DOPED SUPERCONDUCTOR IN GUBSER-ROCHA MODEL

Inspired by ref.[21], we try to construct a holographic superconducting dome in Gubser-Rocha model[36]. We consider the following action (1):

$$S = \int \sqrt{-g} \left[ \mathcal{R} + \frac{6}{L^2} \cosh \varphi - \frac{1}{4} (e^\varphi + Z_A(\chi)) A_{\mu\nu} A^{\mu\nu} - \frac{1}{4} (e^\varphi + Z_B(\chi)) B_{\mu\nu} B^{\mu\nu} - \frac{1}{2} Z_{AB}(\chi) A_{\mu\nu} B^{\mu\nu} - \frac{3}{2} (\partial_\mu \varphi)^2 - H(\chi) (\partial_\mu \theta - q_A A_\mu - q_B B_\mu)^2 - V_{int}(\chi) - \Sigma_{I=x,y} (\partial \phi_I)^2 - \frac{1}{2} (\partial_\mu \chi)^2 \right] d^4x, \quad (1)$$

where we set the gravitational constant  $16\pi G = 1$ . The scalar field  $\varphi$  is the ‘dilaton’ that makes the entropy proportional to temperature near zero temperature. The  $A_{\mu\nu}$  and  $B_{\mu\nu}$  stand for the field strengths of the gauge fields  $A_\mu$  and  $B_\mu$  which provide the finite chemical potentials. We introduce a perturbative charge complex scalar  $\psi = \chi e^{i\theta}$  for superconducting instability,  $\chi$  and  $\theta$  are the amplitude and phase of the charged complex scalar field, respectively.  $Z_A$ ,  $Z_B$  and  $Z_{AB}$  are nontrivial coupling, and  $V_{int}$  is potential term for the scalar field. We will fix these terms later. The two axions  $\phi_I$ :  $\phi_x = mx$ ,  $\phi_y = my$  break the translational invariance.

The corresponding equations of motion with the action (1) are obtained, as follows. The scalar field  $\chi$ ’s equation is

$$\nabla_\mu \nabla^\mu \chi - \partial_\chi V_{int}(\chi) - \frac{1}{4} \partial_\chi Z_A(\chi) A^2 - \frac{1}{4} \partial_\chi Z_B(\chi) B^2 - \frac{1}{2} \partial_\chi Z_{AB}(\chi) A_{\mu\nu} B^{\mu\nu} - \partial_\chi H(\chi) (\partial_\mu \theta - q_A A_\mu - q_B B_\mu)^2 = 0. \quad (2)$$

The equations of motion of the other matter fields are

$$3\nabla_\mu \nabla^\mu \varphi + \frac{6}{L^2} \sinh \varphi - \frac{1}{4} e^\varphi A^2 - \frac{1}{4} e^\varphi B^2 = 0. \quad (3)$$

$$\nabla_\mu [(e^\varphi + Z_A) A^{\mu\nu}] + \nabla_\mu [(e^\varphi + Z_{AB}) B^{\mu\nu}] + 2q_A H(\chi) (\partial^\nu \theta - q_A A^\nu - q_B B^\nu) = 0, \quad (4)$$

$$\nabla_\mu [(e^\varphi + Z_B) B^{\mu\nu}] + \nabla_\mu [(e^\varphi + Z_{AB}) A^{\mu\nu}] + 2q_B H(\chi) (\partial^\nu \theta - q_A A^\nu - q_B B^\nu) = 0, \quad (5)$$

and  $\nabla_\mu \nabla^\mu \phi_I = 0$  for the axions. The Einstein’s equation is given by

$$\begin{aligned} \mathcal{R}_{\mu\nu} - \frac{1}{2} (e^\varphi + Z_A) A_\mu^\beta A_{\nu\beta} - \frac{1}{2} (e^\varphi + Z_B) B_\mu^\beta B_{\nu\beta} - \frac{1}{2} Z_{AB} (g^{\alpha\beta} A_{\mu\beta} B_{\nu\alpha} + g^{\alpha\beta} B_{\mu\beta} A_{\nu\alpha}) \\ - \frac{1}{2} \partial_\mu \chi \partial_\nu \chi - H(\chi) (\partial_\mu \theta - q_A A_\mu - q_B B_\mu) (\partial_\nu \theta - q_A A_\nu - q_B B_\nu) - \frac{3}{2} \partial_\mu \varphi \partial_\nu \varphi - \sum_{I=x,y} \partial_\mu \phi_I \partial_\nu \phi_I \\ - \frac{1}{2} g_{\mu\nu} \left[ \mathcal{R} + \frac{6}{L^2} \cosh \varphi - \frac{1}{4} (e^\varphi + Z_A(\chi)) A_{\mu\nu} A^{\mu\nu} - \frac{1}{4} (e^\varphi + Z_B(\chi)) B_{\mu\nu} B^{\mu\nu} - \frac{1}{2} Z_{AB}(\chi) A_{\mu\nu} B^{\mu\nu} \right. \\ \left. - \frac{3}{2} (\partial_\mu \varphi)^2 - H(\chi) (\partial_\mu \theta - q_A A_\mu - q_B B_\mu)^2 - V_{int}(\chi) - \Sigma_{I=x,y} (\partial \phi_I)^2 - \frac{1}{2} (\partial_\mu \chi)^2 \right] = 0. \end{aligned} \quad (6)$$

In the following part, the couplings and potential are considered as:

$$Z_A(\chi) = \frac{a\chi^2}{2}, \quad Z_B(\chi) = \frac{b\chi^2}{2}, \quad Z_{AB}(\chi) = \frac{c\chi^2}{2}, \quad H(\chi) = \frac{n\chi^2}{2}, \quad V_{int}(\chi) = \frac{M^2\chi^2}{2}. \quad (7)$$

And we define the  $U(1)_{A,B}$  charges to be:

$$q_A = 1, \quad q_B = 0. \quad (8)$$

Although this value is very specific, Kiritsis et al. have verified that this is feasible[20].

To obtain the solutions for this holographic system (1), we assume the metric ansatz is

$$\begin{aligned} ds^2 &= -f(r)dt^2 + \frac{dr^2}{f(r)} + g(r) (dx^2 + dy^2), \\ A_t &= A_t(r), \quad B_t = B_t(r), \\ \phi_x &= mx, \quad \phi_y = my, \\ \varphi &= \varphi(r), \quad \chi = \chi(r), \quad \theta \equiv 0. \end{aligned} \quad (9)$$

Where  $x, y$  are spatial coordinates on the boundary and  $r$  denotes the radial bulk coordinate. The boundary is located at  $r \rightarrow \infty$ , the horizon is located at  $r = r_0$ . The Hawking temperature of the black brane is given by

$$T = \frac{f'(r)}{4\pi} \Big|_{r_0}. \quad (10)$$

### III. CONDUCTIVITIES IN THE NORMAL PHASE

In normal phase ( $\chi \equiv 0$ ), this model admits the following solution[44],

$$\begin{aligned} \varphi(r) &= \frac{1}{2} \ln(1 + Q/r), \quad g(r) = r^{1/2} (r + Q)^{3/2}, \\ f(r) &= r^{1/2} (r + Q)^{3/2} \left( 1 - \frac{(\mu_A^2 + \mu_B^2)(Q + r_0)^2}{3Q(r + Q)^3} - \frac{m^2}{(r + Q)^2} \right), \\ A_t(r) &= \mu_A \left( 1 - \frac{r_0 + Q}{r + Q} \right), \quad B_t(r) = \mu_B \left( 1 - \frac{r_0 + Q}{r + Q} \right), \\ \phi_x &= mx, \quad \phi_y = my, \end{aligned} \quad (11)$$

where  $r_0$  denotes the horizon radius,  $m$  denotes a strength of the momentum relaxation,  $Q$  is a physical parameter. The density of the charge carriers is denoted by  $\rho_A = \mu_A(Q + r_0)$ , which is dual to the gauge field  $A_\mu$ , while the density of doped charge  $\rho_B = \mu_B(Q + r_0)$  is dual to the gauge field  $B_\mu$ . The doping ratio is given by:

$$x = \frac{\rho_B}{\rho_A} = \frac{\mu_B}{\mu_A}. \quad (12)$$

The chemical potential  $\mu_A$  satisfies the following equation,

$$\mu_A = \sqrt{\frac{3Q(Q + r_0)}{1 + x^2} \left( 1 - \frac{m^2}{(Q + r_0)^2} \right)}. \quad (13)$$

The Hawking temperature is given by

$$T = r_0^{\frac{1}{2}} \frac{\left( 3(Q + r_0)^2 - m^2 \right)}{4\pi (Q + r_0)^{\frac{3}{2}}}. \quad (14)$$

We consider the momentum dissipation and calculate AC/DC conductivities of the our model. Because of the symmetry of the x-y plane, without loss of generality, we only consider the disturbance in the  $x$  direction. The system includes two  $U(1)$  fields  $A$  and  $B$  as whose dual operators in the boundary theory denoted as  $J_A$  and  $J_B$  describing two currents, respectively. We also write corresponding external electric fields and conductivities as  $E_A$ ,  $E_B$  and  $\sigma_A$ ,  $\sigma_B$ , respectively. In general, the external field  $E_A$  also contributes to the current  $J_B$ . This process is reciprocal. The associated conductivity is called as  $\gamma_{AB}$ .  $\sigma_A$  and  $\sigma_B$  are interpreted as electric conductivity and spin-spin conductivity, and relatively  $\gamma_{AB}$  is spin conductivity[25]. The heat current  $\mathcal{Q}$  is also coupled with these two currents. They satisfy Ohm's law, which is expressed as

$$\begin{pmatrix} J_A \\ \mathcal{Q} \\ J_B \end{pmatrix} = \begin{pmatrix} \sigma_A & \alpha T & \gamma \\ \alpha T & \kappa T & \beta T \\ \gamma & \beta T & \sigma_B \end{pmatrix} \begin{pmatrix} E_A \\ -\nabla T/T \\ E_B \end{pmatrix}, \quad (15)$$

where  $\kappa$  is the thermal conductivity.  $\alpha$  and  $\beta$  are called as thermo-electric and thermospin conductivities, respectively. This non-diagonal matrix is symmetric as a result of the time-reversal symmetry. We compute the conductivities  $\sigma_A$ ,  $\gamma$  and  $\sigma_B$  in the normal phase of this system. We will discuss the details in the following subsections.

#### A. DC conductivities

Using the methods in [45], we obtain analytic expressions for the several DC conductivities in the normal phase:

$$\sigma_A = e^\varphi + \frac{r^{1/2}(r + Q)^{3/2} A_t'^2(r)}{2m^2} e^{2\varphi} \Big|_{r=r_0}, \quad (16)$$

$$\sigma_B = e^\varphi + \frac{r^{1/2}(r+Q)^{3/2}B_t'^2(r)}{2m^2}e^{2\varphi}\Big|_{r=r_0}, \quad (17)$$

$$\gamma_{AB} = \frac{r^{1/2}(r+Q)^{3/2}A_t'(r)B_t'(r)}{2m^2}e^{2\varphi}\Big|_{r=r_0}. \quad (18)$$

For convinience, we definite scaled variables by

$$\tilde{Q} := \frac{Q}{r_0}, \quad \tilde{m} := \frac{m}{r_0}, \quad \tilde{T} := \frac{T}{r_0}, \quad \tilde{\mu} := \frac{\mu}{r_0}. \quad (19)$$

We also define two physical dimensionless quantities[13]:

$$\bar{T} := \frac{\tilde{T}}{\tilde{\mu}} = \frac{3(1+\tilde{Q})^2 - \tilde{m}^2}{4\sqrt{3}\pi\sqrt{\frac{\tilde{Q}(1+\tilde{Q})^2}{1+x^2}((1+\tilde{Q})^2 - \tilde{m}^2)}}, \quad (20)$$

$$\bar{m} := \frac{\tilde{m}}{\tilde{\mu}} = \sqrt{\frac{(1+\tilde{Q})\tilde{m}^2}{\frac{3\tilde{Q}}{1+x^2}((1+\tilde{Q})^2 - \tilde{m}^2)}}. \quad (21)$$

Using (20),(21), one can express  $\tilde{Q}$  as a function of  $\bar{T}$  and  $\bar{m}$ , i.e.,  $\tilde{Q}(\bar{T}, \bar{m})$ . The DC conductivities (16)-(18) are expressed in terms of  $\tilde{Q}$ ,  $\bar{m}$  and  $x$  as

$$\sigma_A = \sqrt{1+\tilde{Q}} + \frac{\sqrt{1+\tilde{Q}}}{2\bar{m}^2}, \quad (22)$$

$$\sigma_B = \sqrt{1+\tilde{Q}} + x^2 \frac{\sqrt{1+\tilde{Q}}}{2\bar{m}^2}, \quad (23)$$

$$\gamma_{AB} = x \frac{\sqrt{1+\tilde{Q}}}{2\bar{m}^2}. \quad (24)$$

The conductivity  $\sigma_A$  can be divided into the following two cases by the values of  $\bar{T}$  and  $\bar{m}$ .

$$\tilde{Q} \sim \frac{3(1+2\bar{m}^2)^2}{16\pi^2(1+3\bar{m}^2)\bar{T}^2} \quad (\bar{T} \ll 1 \text{ for given } \bar{m}), \quad \sigma_A \sim \frac{\sqrt{3}(1+2\bar{m}^2)^2}{8\pi\bar{m}^2\sqrt{1+3\bar{m}^2}} \frac{1}{\bar{T}}, \quad (25)$$

$$\tilde{Q} \sim \frac{\bar{m}^2}{4\pi^2\bar{T}^2} \quad (\bar{m} \gg 1 \text{ for given } \bar{T}), \quad \sigma_A \sim \frac{\bar{m}}{2\pi\bar{T}}. \quad (26)$$

As can be seen from the above equation, the resistivity ( $\rho = 1/\sigma_A$ ) of this model is proportional to temperature in some limits.

## B. AC conductivities

For calculating AC conductivities numerically, we turn on the bulk fluctuations for  $A_x$ ,  $B_x$  and  $g_{tx}$  around the background (11), which serve as the sources for the currents  $J_x^A$  and  $J_x^B$ , as well as the stress energy tensor component  $T_{tx}$  in the dual boundary field theory. Here, we fix the gauge by  $g_{rx} = 0$ . For our purpose, we assume that the fluctuations depend only on  $t$  and  $r$  coordinates. In a case with the momentum dissipations, the axions are also coupled with those fluctuations. By virtue of the symmetry, we consider only the fluctuation for  $\phi_x$ . We consider the ansatz of the fluctuations as

$$\delta A_x(t, r) = \int_{-\infty}^{\infty} \frac{d\omega}{2\pi} e^{-i\omega t} a_x(\omega, r), \quad (27)$$

$$\delta B_x(t, r) = \int_{-\infty}^{\infty} \frac{d\omega}{2\pi} e^{-i\omega t} b_x(\omega, r), \quad (28)$$

$$\delta \phi_x(t, r) = \int_{-\infty}^{\infty} \frac{d\omega}{2\pi} e^{-i\omega t} \Phi_x(\omega, r), \quad (29)$$

$$\delta g_{tx}(t, r) = \int_{-\infty}^{\infty} \frac{d\omega}{2\pi} e^{-i\omega t} \frac{r^2}{r_0^2} h_{tx}(\omega, r). \quad (30)$$

We obtain five equations by linearising the full equations of motion (see Appendix A for details) but only four are independent due to the gauge symmetry in the system. We impose the incoming boundary condition on the fluctuations for solving the equations of motion. Near the horizon, the solutions are expanded as

$$\begin{aligned} a_x &= (r - r_0)^\lambda \left( a_x^{(I)} + a_x^{(II)}(r - r_0) + \dots \right), \\ b_x &= (r - r_0)^\lambda \left( b_x^{(I)} + b_x^{(II)}(r - r_0) + \dots \right), \\ \Phi_x &= (r - r_0)^\lambda \left( \Phi_x^{(I)} + \Phi_x^{(II)}(r - r_0) + \dots \right), \\ h_{tx} &= (r - r_0)^{\lambda+1} \left( h_{tx}^{(I)} + h_{tx}^{(II)}(r - r_0) + \dots \right), \end{aligned} \quad (31)$$

where  $\lambda = \frac{i(Q+r_0)\omega}{m^2-3(Q+r_0)^2} \sqrt{1 + \frac{Q}{r_0}}$ , and it corresponds to the incoming boundary condition. By solving the equations of motion near the horizon, we obtain one constraint on  $h_{tx}^{(I)}, a_x^{(I)}, b_x^{(I)}$  and  $\Phi_x^{(I)}$ , which reduces the degrees of freedom. The reason of this mismatch of the degree of freedom is because of the residual gauge freedom. According to [42], we can fix this mismatch by considering an additional solution along the residual gauge orbit, as follows. In the gauge  $g_{rx} = 0$ , there is a residual gauge transformation generated by the Killing vector  $\xi^\mu = (0, \zeta e^{-i\omega t}, 0, 0)$  with a constant  $\zeta$ . We obtain the Lie derivative of the background solution with the above Killing vector as

$$\mathcal{L}_\xi A_x = \mathcal{L}_\xi B_x = 0, \quad \mathcal{L}_\xi \Phi_x = m \xi^x, \quad \mathcal{L}_\xi g_{tx} = -i\omega g(r) \xi^x. \quad (32)$$

We obtain the additional solution as

$$a_x = 0, \quad b_x = 0, \quad \Phi_x = m, \quad h_{tx} = -i\omega r_0^2 \left( 1 + \frac{Q}{r} \right)^{3/2}. \quad (33)$$

Note that the above solution does not satisfy the incoming boundary condition at the horizon since it does not corresponds to a physical degree of freedom. One can find further discussion on this in [43]. With the set of the numerical solutions and the additional solution, we can study the linear responses by using the standard shooting method.

Near the boundary ( $r \rightarrow \infty$ ), the asymptotic behaviors of the fluctuations are

$$\begin{aligned} a_x &= a_x^{(0)} + \frac{1}{r} a_x^{(1)} + \dots, \\ b_x &= b_x^{(0)} + \frac{1}{r} b_x^{(1)} + \dots, \\ \Phi_x &= \Phi_x^{(0)} + \frac{1}{r} \Phi_x^{(1)} + \dots, \\ h_{tx} &= h_{tx}^0 + \frac{1}{r^3} h_{tx}^{(1)} + \dots. \end{aligned} \quad (34)$$

According to AdS/CFT theory, the leading terms ( $a_x^{(0)}, b_x^{(0)}, \Phi_x^{(0)}, h_{tx}^0$ ) correspond to the sources and the subleading terms ( $a_x^{(1)}, b_x^{(1)}, \Phi_x^{(1)}, h_{tx}^{(1)}$ ) would be considered as the response terms. We calculate AC conductivities numerically by using these terms. Because the linearized equations of the two gauge fields are coupled with each other, the two currents  $J_A^x$  and  $J_B^x$  have an overlap. The overlap leads to spin conductivity  $\gamma$ . Using the holographic dictionary, we

numerically calculate the AC conductivities by the following formulas [24]

$$\begin{aligned}\sigma_A &= \frac{J_A}{E_A} \bigg|_{\nabla T=E_B=0} = - \frac{i}{\omega} \frac{a_x^{(1)}}{a_x^{(0)}} \bigg|_{g_{tx}^{(0)}=b_x^{(0)}=0}, \\ \sigma_B &= \frac{J_B}{E_B} \bigg|_{\nabla T=E_A=0} = - \frac{i}{\omega} \frac{b_x^{(1)}}{b_x^{(0)}} \bigg|_{g_{tx}^{(0)}=a_x^{(0)}=0}, \\ \gamma &= \frac{J_B}{E_A} \bigg|_{\nabla T=E_B=0} = - \frac{i}{\omega} \frac{b_x^{(1)}}{a_x^{(0)}} \bigg|_{g_{tx}^{(0)}=b_x^{(0)}=0}.\end{aligned}\tag{35}$$

We also impose  $\Phi_x^{(0)} = 0$  for obtaining correct conductivities. In the following, we divide the calculation of AC conductivities into two cases depending on whether momentum dissipation exists or not. We compare them and study the effect on conductivity after breaking translational symmetry.

### 1. A case without momentum dissipation

First, we study the AC conductivity in a case without momentum dissipation,  $m = 0$ , i.e., the system preserves the translational invariance. Here, we set  $r_0 = 1$  for simplicity. As reported in a different two-currents model [24], our system also enjoys the symmetry about  $x$ :

$$\sigma_A(x, \omega) = \sigma_B\left(\frac{1}{x}, \omega\right), \quad \gamma(x, \omega) = \gamma\left(\frac{1}{x}, \omega\right)\tag{36}$$

We have checked the above symmetry numerically. See Appendix B for details.

We fix  $Q = 1$ , and compare the effects of different doping parameters  $x$  on the conductivity. Figure 1 shows the AC conductivity for various  $x$  in a case without momentum dissipation. In Figure 1, we find that with the increase of doping  $x$ , the asymptotic value of real part of the conductivity at  $\omega = 0$  also increases due to the increases of the density of carriers. Remark that the DC conductivity is actually infinite due to the presence of the Dirac delta at  $\omega = 0$  in this case. According to [46], such a finite part of the real part of the conductivity in the vicinity of  $\omega = 0$  can be understood as the incoherent conductivity  $\sigma_Q$ .

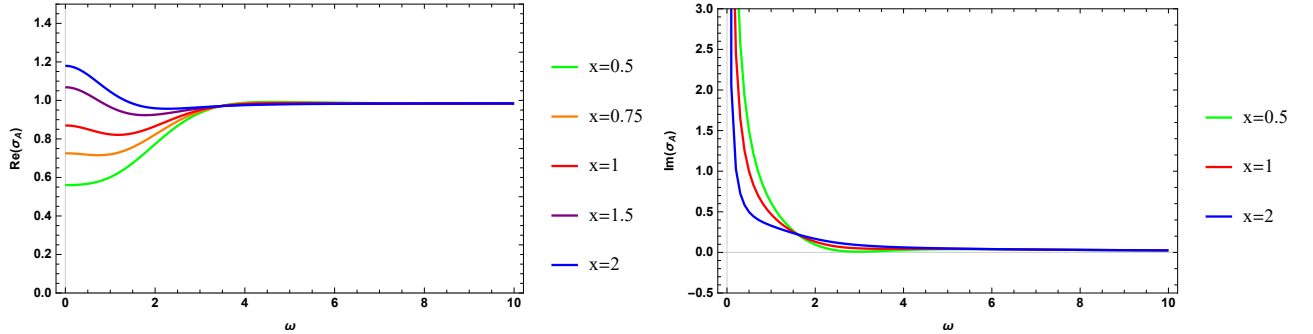


FIG. 1: The real part(left) and the imaginary part(right) of the electric conductivity  $\sigma_A$ . The temperature is fixed at  $T = 0.338$ .

### 2. A case with momentum dissipation

Next, we consider the case where momentum dissipation is introduced, i.e.  $m \neq 0$ . Although the translational symmetry has been broken due to the presence of the axions, the symmetry of the system in the normal phase still exist. Our results show the conductivities  $\sigma_A$ ,  $\sigma_B$  and  $\gamma$  satisfy the symmetry (36), see Appendix B for details.

We fix  $m = 1$  and compare the effect of increasing  $x$  on the conductivity  $\sigma_A$  in Figure 2. Due to the presence of the momentum dissipation, the Drude peak is broaden and the DC conductivity becomes the finite value given by (16).

We have calculated the DC limit of the numerics at  $\omega = 0$  agrees with the analytic value  $\sigma_A$  in (16). Our results show that, unlike the case where momentum dissipation is not introduced, the conductivities  $\sigma_A$  decrease with the increase of  $x$ . This observation is very interesting, and we consider that it is the result of competition between the momentum dissipation that breaks the translational symmetry and the chemical potential.

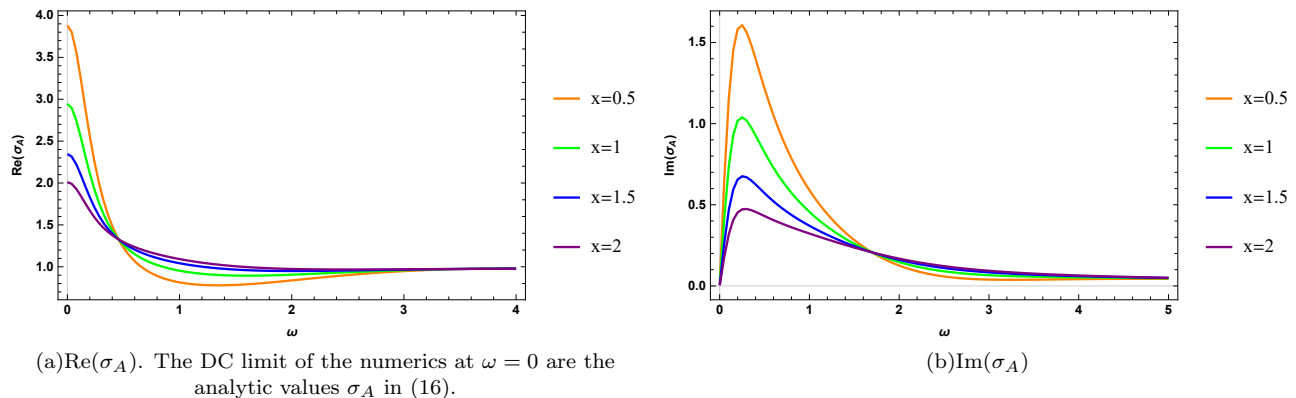


FIG. 2: The conductivities  $\sigma_A$  change with the different doping parameter  $x$  at  $m = 1$ . The temperature is fixed at  $T = 0.310$ .

Figure 3 shows how the conductivity  $\sigma_A$  changes with the dissipation intensity  $m$  at  $x = 2$ . Figure 3(a) is the real part and Figure 3(b) is the imaginary part of the conductivity  $\sigma_A$ . We find that as  $m$  increases, the value of  $\text{Re}(\sigma_A)$  at  $\omega = 0$  is smaller and the Drude peak disappears.

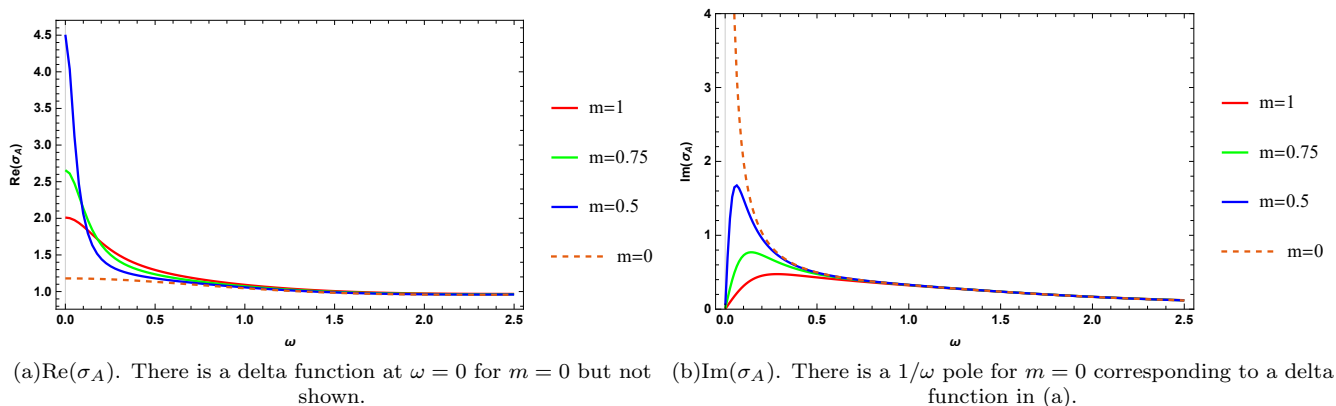


FIG. 3: The conductivities  $\sigma_A$  change with the different dissipation intensity  $m$  at  $T = 0.310, 0.322, 0.331, 0.338$  (red, green, blue, dashed).

#### IV. THE SUPERCONDUCTING DOME

In this section, we investigate the phase diagram in  $x$ - $T$  plane in our model. At the critical temperature, the spontaneous breaking of  $U(1)$  symmetry is dual to the condensation of scalar field  $\chi$  in the bulk. And the superconducting instability corresponds to developing a non-trivial scalar  $\chi$ . In order to investigate whether the boundary system exhibits a superconducting phase, we study the instability of the scalar hair around the normal phase of the dual bulk system. We solve the linearized equation of motion about  $\chi$  in the background of (11).

The phase transition is related to the formation of scalar hair around the normal phase. When the temperature is below the critical temperature  $T_c$ , the system becomes unstable and the scalar hair begins to develop. In the vicinity of the temperature at which the system develops non-trivial scalar hair of  $\chi$ , the value of  $\chi$  should be small so we can consider it as a perturbation. Then we solve the linear motion equation (2) of the scalar field  $\chi$  in the normal phase

background without taking backreaction into consideration. By making a coordinate transformation of the metric form (11) i.e.  $u = 1/r$ , (2) yields

$$\chi'' + \left( \frac{f'}{f} + \frac{g'}{g} - \frac{2}{u} \right) \chi' + \frac{\chi \left( f \left( au^2 A_t'^2 + bu^2 B_t'^2 + 2cu^2 A_t' B_t' - \frac{2M^2}{u^2} \right) + 2n(q_A A_t + q_B B_t)^2 \right)}{2f^2} = 0. \quad (37)$$

where ‘prime’ stands for  $\partial_u$ .

To solve the equation (37), we need to impose appropriate boundary conditions. In the IR limit, near the horizon, we impose the regular condition for the scalar field, it can be expressed as

$$\chi(u) = \chi_h^0 + \chi_h^{(1)}(u - u_h) + \frac{\chi_h^{(2)}}{2!}(u - u_h)^2 + \dots. \quad (38)$$

In the UV, near  $u = 0$ ,  $\chi$  has an asymptotic expansion of

$$\chi(u) = \chi^{(-)}u^{3-\Delta} + \chi^{(+)}u^{\Delta} + \dots, \quad (39)$$

where the scaling dimension  $\Delta = 5/2$ . We also impose a condition to vanish the nonnormalizable term. As a result, the solution of this two-points boundary values problem is a static zero mode which indicates onset of the instability.

We fix the parameters in (7) and  $m$ ,  $Q$ , leaving with only two state parameters, the doping  $x$  and the temperature  $T_c$ . We look for the temperature maximum corresponding to the horizon radius  $u_h$  at which the source coefficient  $\chi^{(-)}$  of the field  $\chi$  near the boundary expansion disappears. Therefore, given  $x$ , we hope to find a solution that satisfies the two boundary conditions above, which is a static zero mode of superconducting developmental instability.

On such terms we test a set of parameters with the following values:

$$a = -10, b = -\frac{4}{3}, c = 14, n = 1, Q = 1, M^2 = -\frac{5}{4}. \quad (40)$$

We plot the critical temperature as a function of the doping parameter  $x$  and draw the phase diagram of the  $x$ - $T$  plane with translational symmetry breaking parameter  $m = 0.5$ , as shown in Figure 4. It can indeed be seen that in the case of finite temperature, the critical temperature  $T_c$  obtained by numerical calculation first increases and then decreases with the increase of doping, which is in line with the phase diagram characteristics of high temperature superconductors in reality. The introduction of translational symmetry breaking does not destroy the original superconducting dome structure.

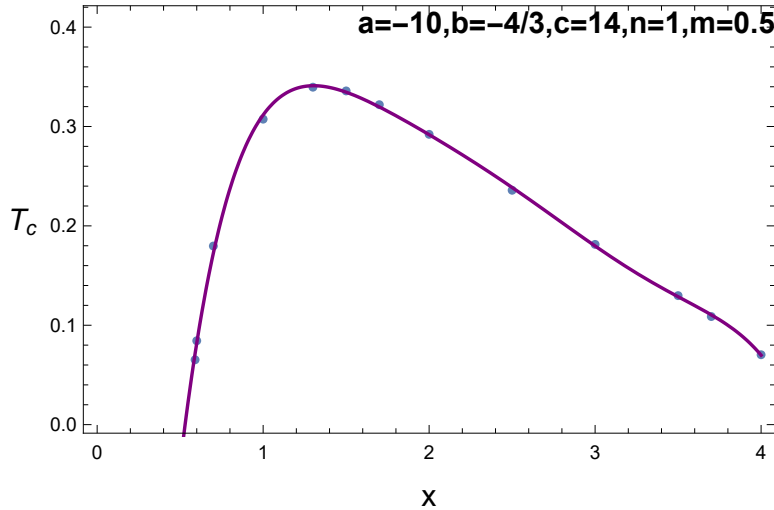


FIG. 4: The phase diagram of the  $(x, T)$  plane of the model (40) at finite temperature when the translational symmetry breaking parameter is  $m = 0.5$ . The dots come directly from our numerical calculations.

We also discuss the influence of the value of  $c$  on dome and obtain the same results as those obtained in [22]. We fix  $a = b = 0$ ,  $m = 0$  and choose different  $c$ . The result is shown in Figure 5. Our result indicates that the higher the value of  $c$ , the larger the dome. The action brought by the coupling of the two gauge fields is obviously the decisive factor leading to the emergence of dome.

With breaking translational symmetry, we reproduce the high- $T_c$  superconducting dome in a black brane whose entropy is proportional to temperature near zero temperature and prove even if the coupling to a single gauge field is zero, relying on cross term coupling, we can still obtain a superconducting dome. This is the main result of our paper.

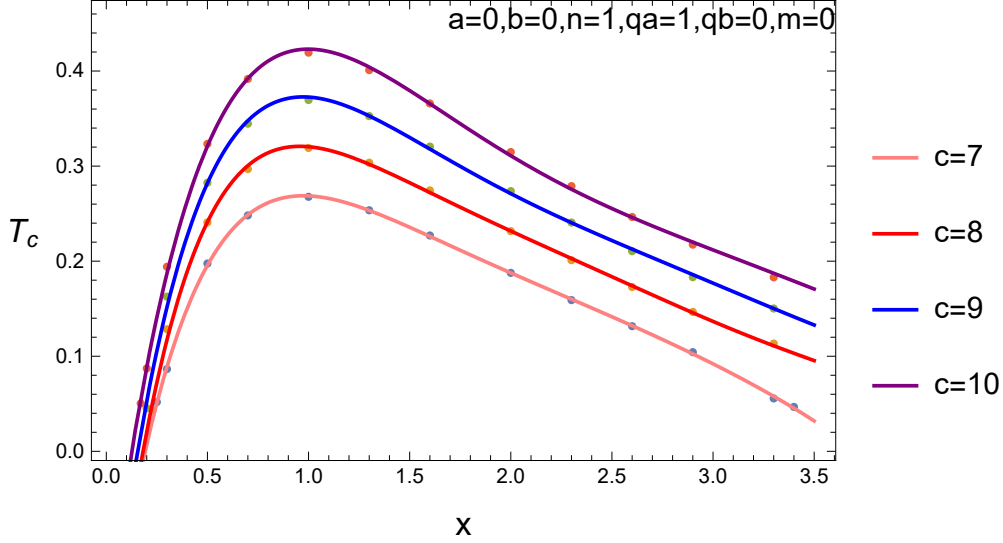


FIG. 5: The phase diagram of the  $(x, T_c)$  plane. We fix  $a = b = 0$ ,  $m = 0$  and choose different  $c$ . The higher the value of  $c$ , the larger the dome.

## V. CONCLUSION AND DISCUSSION

In this paper, We studied the holographic theory of building a dome region in the temperature-doping plane like a realistic high- $T_c$  superconductor. We attempt to realize a superconducting dome on the  $(x, T_c)$  phase diagram in the holographic superconductors model, the Gubser-Rocha model. We first calculate the DC conductivities in the normal phase analytically. Our results show the resistivity is proportional to temperature with the momentum dissipation in normal phase. We then calculate conductivities associated to two gauge fields of our model in the normal phase numerically. We find there is a symmetry between  $\sigma_A$ ,  $\gamma$  and  $\sigma_B$  with specific doping parameter  $x$  in normal phase. Our results indicates momentum dissipation can not break this symmetry.

We furthermore investigate the phase diagram for the normal and superconducting phases. One of the main progress of this paper is to show that the superconducting dome-shaped region exists in the Gubser-Rocha model with broken translational symmetry. This is a generalization of the previous work[22]. Moreover, our results show that larger coupling  $c$  makes the dome higher in this background, which also verified the role of the three point interaction  $-c\chi^2 A_{\mu\nu} B^{\mu\nu}$  under hyperscaling violation geometry.

We have constructed a holographic s-wave doped superconductor closer to the realistic background in a Gubser-Rocha black brane whose entropy is proportional to temperature near zero temperature. Yet most unconventional superconductors have d-wave symmetry, we hope to extend the present work to d-wave holographic superconductor in the future. It would be interesting to follow the lines that we are studying here.

### Appendix A : The linearised equations in momentum space

In this section, we write the linearised equations of motion for the fluctuations studied in section 3. These are obtained as

$$\frac{\omega^2 a_x(r)}{f(r)^2} + \frac{a'_x(r)f'(r)}{f(r)} + a'_x(r)\varphi'(r) + \frac{r^2 h'_{tx}(r)A'_t(r)}{r_0^2 f(r)} + a''_x(r) + h_{tx}(r) \left( \frac{2rA'_t(r)}{r_0^2 f(r)} + \frac{r^2 \varphi'(r)A'_t(r)}{r_0^2 f(r)} + \frac{r^2 A''_t(r)}{r_0^2 f(r)} \right) = 0, \quad (41)$$

$$\frac{\omega^2 b_x(r)}{f(r)^2} + \frac{b'_x(r)f'(r)}{f(r)} + b'_x(r)\varphi'(r) + \frac{r^2 h'_{tx}(r)A'_t(r)}{r_0^2 f(r)} + b''_x(r) + h_{tx}(r) \left( \frac{2rB'_t(r)}{r_0^2 f(r)} + \frac{r^2 \varphi'(r)B'_t(r)}{r_0^2 f(r)} + \frac{r^2 B''_t(r)}{r_0^2 f(r)} \right) = 0, \quad (42)$$

$$\Phi_x''(r) + \left(\frac{f'(r)}{f(r)} + \frac{g'(r)}{g(r)}\right)\Phi_x'(r) + \frac{\omega^2}{f(r)^2}\Phi_x(r) - \frac{imr^2\omega h_{tx}(r)}{r_0^2 f(r)^2 g(r)} = 0, \quad (43)$$

$$h_{tx}(r) \left(\frac{2}{r} - \frac{g'(r)}{g(r)}\right) + h_{tx}'(r) + \frac{e^{\varphi(r)} r_0^2}{r^2} (a_x(r)A_t'(r) + b_x(r)B_t'(r)) + \frac{2imr_0^2 f(r)\Phi_x'(r)}{r^2 \omega} = 0, \quad (44)$$

$$\begin{aligned} h_{tx}''(r) + \frac{4h_{tx}'(r)}{r} + \frac{e^{\varphi(r)} r_0^2}{r^2} (a_x'(r)A_t'(r) + b_x'(r)B_t'(r)) - \frac{2imr_0^2 \omega}{r^2 f(r)} \Phi_x(r) \\ + h_{tx}(r) \left(\frac{2}{r^2} + \frac{3}{f(r)}(e^{-\varphi(r)} + e^{\varphi(r)}) - \frac{f'(r)g'(r)}{f(r)g(r)} + \frac{g'(r)^2}{2g(r)^2} - \frac{3}{2}\varphi'(r)^2 \right. \\ \left. + \frac{e^{\varphi(r)}}{2f(r)}(A_t'(r)^2 + B_t'(r)^2) - \frac{f''(r)}{f(r)} - \frac{2g''(r)}{g(r)} - \frac{2m^2}{f(r)g(r)}\right) = 0. \end{aligned} \quad (45)$$

The last equation can be obtained from the others. Thus, the set of the independent equations are given by (41), (42), (43) and (44).

### Appendix B : Symmetry between conductivities in normal phase

In this section, we present electrical conductivity in our model that support the conclusions that the conductivities  $\sigma_A$ ,  $\sigma_B$  and  $\gamma$  satisfy the symmetry (36) in Section III. In the case of no momentum dissipation, we show the real part of the conductivity  $\sigma_A$  and  $\sigma_B$  at  $x = 1$  in Figure 6(a),  $\gamma$  at  $x=0.5$  and  $x=2$  in Figure 6(b), respectively. Figure 7 shows images of the conductivities with the momentum dissipation parameter  $m = 1$ . The fact that two lines coincide perfectly prove the symmetry of the system still exists after the translation symmetry is broken.

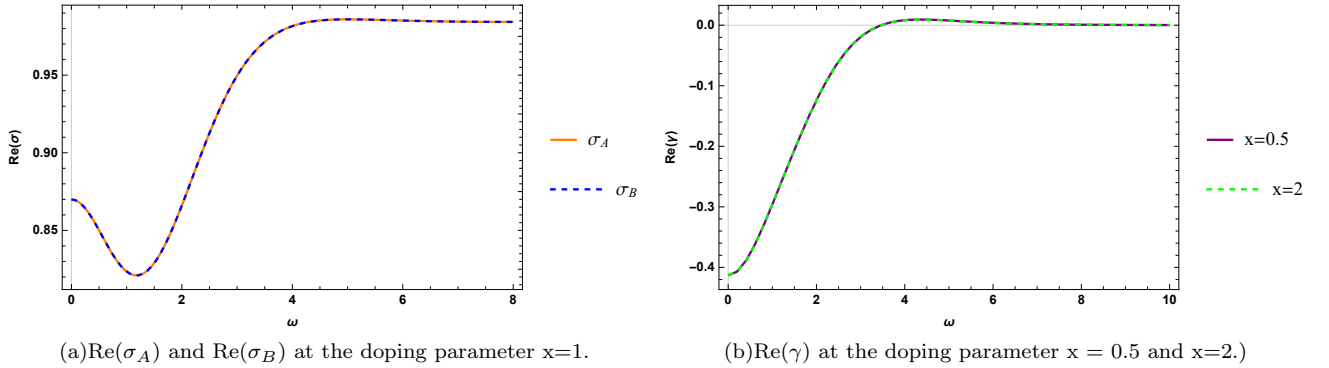


FIG. 6: A case without momentum dissipation  $m = 0$  at  $T = 0.338$ , the two lines coincide perfectly. The system enjoys the symmetry. There is a delta function at  $\omega = 0$  but not shown.

### Acknowledgements

We would like to thank Xian-Hui Ge, Sang-Jin Sin, Blaise Gout  raux and Li Li for valuable comments and discussions. This work is supported by NSFC China (Grants No. 12275166, No. 11875184, No. 12147158 and No. 11805117).

- 
- [1] E. W. Carlson, V. J. Emery, S. A. Kivelson, and D. Orgad. Concepts in high temperature superconductivity, 2002.
  - [2] Juan Maldacena. *International Journal of Theoretical Physics*, 38(4):1113–1133, 1999.

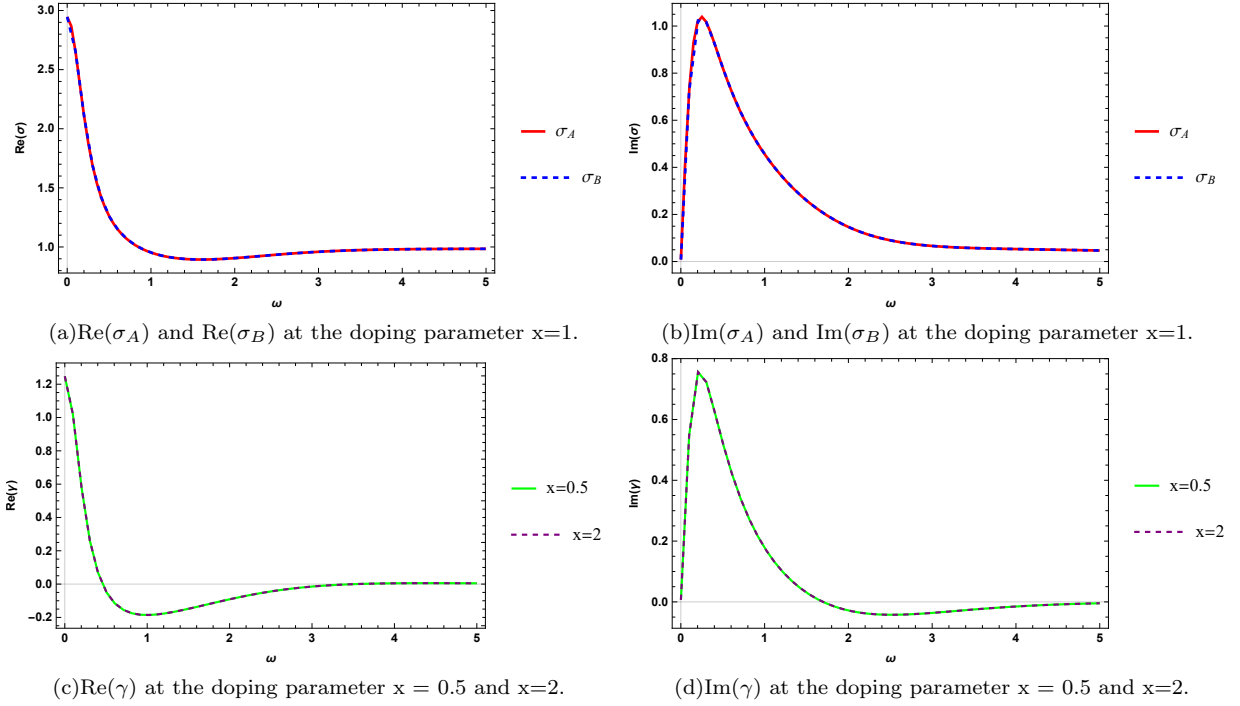


FIG. 7: A case with momentum dissipation  $m = 1$  at  $T = 0.310$ , the two lines coincide perfectly. The system still enjoys the symmetry.

- [3] S.S. Gubser, I.R. Klebanov, and A.M. Polyakov. Gauge theory correlators from non-critical string theory. *Physics Letters B*, 428(1-2):105–114, may 1998.
- [4] Edward Witten. Anti de sitter space and holography, 1998.
- [5] G. 't Hooft. Dimensional reduction in quantum gravity, 2009.
- [6] Sean A. Hartnoll, Andrew Lucas, and Subir Sachdev. Holographic quantum matter, 2018.
- [7] Jan Zaanen, Yan Liu, Ya-Wen Sun, and Koenraad Schalm. *Holographic duality in condensed matter physics*. Cambridge University Press, 2015.
- [8] Sean A Hartnoll, Christopher P Herzog, and Gary T Horowitz. Holographic superconductors. *Journal of High Energy Physics*, 2008(12):015–015, dec 2008.
- [9] Sean A. Hartnoll, Christopher P. Herzog, and Gary T. Horowitz. Building a holographic superconductor. *Phys. Rev. Lett.*, 101:031601, Jul 2008.
- [10] Rong gen Cai, Li Li, Li fang Li, and Run-Qiu Yang. Introduction to holographic superconductor models. *Science China Physics, Mechanics & Astronomy*, 58:1–46, 2015.
- [11] Sean A. Hartnoll, Joseph Polchinski, E. Silverstein, and David Tong. Towards strange metallic holography. *Journal of High Energy Physics*, 2010:1–54, 2010.
- [12] Bom Soo Kim, Elias Kiritsis, and Christos Panagopoulos. Holographic quantum criticality and strange metal transport. *New Journal of Physics*, 14, 2012.
- [13] Hyun-Sik Jeong and Keun-Young Kim. Homes’ law in holographic superconductor with linear- $t$  resistivity. *Journal of High Energy Physics*, 2022(3), mar 2022.
- [14] Hyun-Sik Jeong, Chao Niu, and Keun-Young Kim. Linear- $t$  resistivity at high temperature. *Journal of High Energy Physics*, 2018(10), oct 2018.
- [15] Shesansu Sekhar Pal. Model building in ads/cmt: Dc conductivity and hall angle. *Physical Review D*, 84:126009, 2011.
- [16] Yongjun Ahn, Matteo Baggioli, Hyun-Sik Jeong, and Keun-Young Kim. Holographic gubser-rocha model does not capture all the transport anomalies of strange metals, 2023.
- [17] Jie Yuan, Qihong Chen, Kun Jiang, Zhongpei Feng, Zefeng Lin, Heshan Yu, Ge He, Jinsong Zhang, Xingyu Jiang, Xu Zhang, et al. Scaling of the strange-metal scattering in unconventional superconductors. *Nature*, 602(7897):431–436, 2022.
- [18] Sean A Hartnoll. Lectures on holographic methods for condensed matter physics. *Classical and Quantum Gravity*, 26(22):224002, oct 2009.
- [19] Wenjun Huang, Guoyang Fu, Dan Zhang, Zhenhua Zhou, and Jian-Pin Wu. Doped holographic fermionic system. *The European Physical Journal C*, 80(7), jul 2020.
- [20] Elias Kiritsis and Li Li. Holographic competition of phases and superconductivity. *Journal of High Energy Physics*, 2016(1), jan 2016.
- [21] Matteo Baggioli and Mikhail Goykhman. Under the dome: doped holographic superconductors with broken translational symmetry. *Journal of High Energy Physics*, 2016(1), jan 2016.
- [22] Wenhe Cai and Sang-Jin Sin. The superconducting dome for holographic doped mott insulator with hyperscaling violation.

*The European Physical Journal C*, 81(6), jun 2021.

- [23] Marek Rogatko and Karol I. Wysokinski. Two interacting current model of holographic dirac fluid in graphene. *Physical Review D*, 97(2), jan 2018.
- [24] Francesco Bigazzi, Aldo L. Cotrone, Daniele Musso, Natalia Pinzani Fokeeva, and Domenico Seminara. Unbalanced holographic superconductors and spintronics, 2012.
- [25] Dan Zhang, Zhenhua Zhou, Guoyang Fu, and Jian-Pin Wu. Conductivities in holographic two-currents model. *Physics Letters B*, 815:136178, 2021.
- [26] Yunseok Seo, Geunho Song, Philip Kim, Subir Sachdev, and Sang-Jin Sin. Holography of the dirac fluid in graphene with two currents. *Physical Review Letters*, 118(3), jan 2017.
- [27] Nevill Francis Mott. The electrical conductivity of transition metals. *Proceedings of the Royal Society of London. Series A-Mathematical and Physical Sciences*, 153(880):699–717, 1936.
- [28] Nevill Francis Mott. The resistance and thermoelectric properties of the transition metals. *Proceedings of the Royal Society of London. Series A-Mathematical and Physical Sciences*, 156(888):368–382, 1936.
- [29] Patrick A Lee, Naoto Nagaosa, and Xiao-Gang Wen. Doping a mott insulator: Physics of high-temperature superconductivity. *Reviews of modern physics*, 78(1):17, 2006.
- [30] Yi Ling, Peng Liu, Chao Niu, and Jian-Pin Wu. Building a doped mott system by holography. *Physical Review D*, 92(8):086003, 2015.
- [31] Nabil Iqbal, Hong Liu, Márk Mezei, and Qimiao Si. Quantum phase transitions in holographic models of magnetism and superconductors. *Physical Review D*, 82(4), aug 2010.
- [32] K Jin, NP Butch, K Kirshenbaum, J Paglione, and RL Greene. Link between spin fluctuations and electron pairing in copper oxide superconductors. *Nature*, 476(7358):73–75, 2011.
- [33] Matteo Baggioli and Oriol Pujolà s. Electron-phonon interactions, metal-insulator transitions, and holographic massive gravity. *Physical Review Letters*, 114(25), jun 2015.
- [34] Shuhang Zhang, Zixu Zhao, Qiyuan Pan, and Jiliang Jing. Excited states of holographic superconductors with hyperscaling violation. *Nuclear Physics B*, 976:115701, 2022.
- [35] Xian-Hui Ge, Yu Tian, Shang-Yu Wu, and Shao-Feng Wu. Hyperscaling violating black hole solutions and magnetothermoelectric dc conductivities in holography. *Physical Review D*, 96(4):046015, 2017.
- [36] Steven S. Gubser and Fabio D. Rocha. Peculiar properties of a charged dilatonic black hole in ads 5. *Physical Review D*, 81:046001, 2010.
- [37] Floris Balm, Nicolas Chagnet, Sam Arend, Joost Aretz, Kevin Grosvenor, Martijn Janse, Ole Moors, Jonah Post, Vladimir Ohanesjan, David Rodriguez-Fernandez, Koenraad Schalm, and Jan Zaanen. T-linear resistivity, optical conductivity and planckian transport for a holographic local quantum critical metal in a periodic potential, 2022.
- [38] Jie Ren and Haodong Xie. Holographic superconductors at zero density. *Physical Review D*, 107(10), may 2023.
- [39] Yan Liu, Xi-Jing Wang, Jian-Pin Wu, and Xin Zhang. Alternating current conductivity and superconducting properties of a holographic effective model with broken translations. *The European Physical Journal C*, 82(5), may 2022.
- [40] Yan Liu, Xi-Jing Wang, Jian-Pin Wu, and Xin Zhang. Holographic superconductor with gauge-axion coupling, 2023.
- [41] Guoyang Fu, Huajie Gong, Peng Liu, Xiao-Mei Kuang, and Jian-Pin Wu. Charge transport properties in a novel holographic quantum phase transition model. *The European Physical Journal C*, 83(6):516, 2023.
- [42] Keun-Young Kim, Kyung Kiu Kim, Yunseok Seo, and Sang-Jin Sin. Coherent/incoherent metal transition in a holographic model. *Journal of High Energy Physics*, 2014(12):1–27, 2014.
- [43] Keun-Young Kim, Kyung Kiu Kim, Yunseok Seo, and Sang-Jin Sin. Gauge invariance and holographic renormalization. *Physics Letters B*, 749:108–114, 2015.
- [44] Zhenhua Zhou, Yi Ling, and Jian-Pin Wu. Holographic incoherent transport in einstein-maxwell-dilaton gravity. *Physical Review D*, 94(10), nov 2016.
- [45] Ze-Nan Chen, Xian-Hui Ge, Shang-Yu Wu, Guo-Hong Yang, and Hong-Sheng Zhang. Magnetothermoelectric DC conductivities from holography models with hyperscaling factor in lifshitz spacetime. *Nuclear Physics B*, 924:387–405, nov 2017.
- [46] Richard A Davison, Blaise Goutéraux, and Sean A Hartnoll. Incoherent transport in clean quantum critical metals. *Journal of High Energy Physics*, 2015(10):1–18, 2015.